Core excitations beyond maximally aligned configurations in ^{123}I

Purnima Singh and A. K. Singh

Department of Physics and Meteorology, Indian Institute of Technology Kharagpur, Kharagpur IN-721302, India

A. N. Wilson and J. Rogers

Research School of Physics and Engineering, The Australian National University, Canberra, ACT 0200, Australia

H. Hübel, A. Bürger, and S. Chmel

Helmholtz-Institut für Strahlen- und Kernphysik, Universität Bonn, Nussallee 14-16, D-53115 Bonn, Germany

I. Ragnarsson

Division of Mathematical Physics, LTH, Lund University, Box 118, S-22100 Lund, Sweden

G. Sletten and B. Herskind

Niels Bohr Institute, Blegdamsvej 17, DK-2100 Copenhagen, Denmark

M. P. Carpenter, R. V. F. Janssens, T. L. Khoo, F. G. Kondev, T. Lauritsen, and S. Zhu

Physics Division, Argonne National Laboratory, Argonne, Illinois 60439, USA

A. Korichi and Hoa Ha

CSNSM-IN2P3, F-91405 Orsay Campus, France

P. Fallon

Nuclear Science Division, Lawrence Berkeley National Laboratory, Berkeley, California 94720, USA

B. M. Nyakó and J. Timár

Institute of Nuclear Research of the Hungarian Academy of Sciences, H-4001 Debrecen, Hungary

K. Juhász

Department of Information Technology, University of Debrecen, H-4032, Hungary

High-spin states in ^{123}I have been populated in the ^{80}Se(^{48}Ca,$p4n$)^{123}I reaction at 207 MeV and γ-ray coincidence events have been recorded with the Gammasphere spectrometer. The level scheme of ^{123}I has been extended up to spin $I = 63/2$. The nucleus undergoes a shape transition from moderately deformed states with collective rotation at low spins to noncollective oblate configurations at higher spins. Maximally aligned terminating states involving all nine particles outside the ^{114}Sn core and states with one particle antialigned are identified. A large number of weak transitions feed the terminating states. Cranked Nilsson-Strutinsky calculations have been performed to determine possible configurations for the observed energy levels.

I. INTRODUCTION

The low-energy states of the odd-mass I isotopes ($Z = 53$) are formed by a coupling of the odd proton to the levels of neighboring even-even Te nuclei. Bands of low collectivity are observed up to the medium-spin region. At higher energies, however, these nuclei exhibit a more complex structure with coexisting weakly collective and noncollective quasiparticle-aligned configurations. Energetically favored noncollective oblate states with spins between 39/2 and 63/2 have been observed in odd-A I isotopes [1–11]. In a recent spectroscopic study of ^{125}I, three maximally aligned states involving all eleven particles outside the ^{114}Sn core were observed [11]. In addition to these states, noncollective states with the angular momentum of one and two particles antialigned with respect

to the rotation axis were identified in this nucleus. The number of such antialigned states observed to date is rather limited. The first case was the $I^\pi = 40^+$ state in ^{158}Er [12], where a neutron of $h_{9/2}f_{7/2}$ character is antialigned relative to the maximally aligned configuration with $I^\pi = 46^+$. Similar states were found later also in ^{156}Er, ^{157}Er, and ^{159}Er [13–15]. In the mass-125 region, in addition to ^{125}I, such a state was reported only in ^{121}I [10].

Higher-spin states, beyond the full alignment of the valence particles, can only be created by energetically expensive particle-hole excitations from the core. This type of excitation was observed, e.g., in $^{155-158}$Er [13,16–18], where many weakly populated states, lying between 1.0 and 2.5 MeV above the terminating states, were delineated. Such excitations, feeding maximally aligned states, were also reported in

[121]I [10]. The $A \simeq 160$ and $\simeq 120$ mass regions exhibit certain similarities. Proton particle-hole excitations across the semimagic $Z = 64$ shell gap in the Er isotopes are analogous to neutron excitations across the $N = 64$ core in the $A \simeq 120$ region [19].

A particularly interesting feature of the $A \simeq 120$ region is the occurrence of highly deformed rotational bands extending into the $I = 50$–60 region [20–24]. Their configurations involve neutron and proton excitations across the $N = 82$ and $Z = 50$ shell gaps, respectively. Transition quadrupole moments, estimated from Doppler-shift lifetime results, lie between 4.3 and 5.9 b [21,22].

In the present work, we report on an investigation of the high-spin structure of [123]I. The previously known level scheme [5,25–27] is extended considerably. Maximally aligned valence-space configurations and states with one particle antialigned have been discovered. In addition, a large number of weak, high-energy transitions, probably depopulating core-breaking excited states, have been observed to feed the fully aligned, noncollective levels. Furthermore, three highly deformed collective bands have been found as well. However, they will be discussed in a forthcoming publication [28].

In Sec. II, the experimental setup and the data analysis are briefly described. The experimental results and the ^{123}I level scheme are presented in Sec. III, followed by a discussion of the results within the framework of the cranked Nilsson-Strutinsky (CNS) model in Sec. IV. A brief summary of the present work is given in Sec. V.

II. EXPERIMENTAL DETAILS AND DATA ANALYSIS

High-spin states in ^{123}I were populated in the heavy-ion fusion-evaporation reaction $^{80}\text{Se}(^{48}\text{Ca},p4n)^{123}\text{I}$. The ^{48}Ca beam of 207 MeV was provided by the ATLAS accelerator at Argonne National Laboratory. The target consisted of a 0.6 mg/cm^2 layer of ^{80}Se evaporated on a 0.3 mg/cm^2 Au backing. The Se foil was protected by a 0.04 mg/cm^2 Au layer. The target was mounted on a rotating wheel and the beam was slightly defocused and wobbled horizontally. With these precautions it could withstand a beam intensity of 4 pnA without damage over the time of the experiment. Gamma-ray coincidences were measured with the Gammasphere spectrometer [29] consisting of 101 Compton-suppressed Ge detectors. In a beam time of 10 days, a total of 2.7×10^9 events, with a Ge-detector coincidence fold $\geqslant 4$ were collected. Although the main motivation of the experiment was to search for hyperdeformed structures in ^{124}Xe, excited states in ^{123}I were populated with sufficient intensity to motivate the present study.

In the off-line analysis, the coincidence events were sorted into γ-γ matrices, γ-γ-γ cubes and γ-γ-γ-γ hypercubes. The software package RADWARE [30] was used for the data analysis. To determine angular distribution ratios, R_θ, the coincidence events were sorted into two matrices. One matrix contained events detected at forward and backward (fb) angles, close to average positions of $35°$ and $145°$, respectively, on one axis and all events (all) on the other axis. The second matrix contained events detected close

to $90°$ (90) on one axis and all events on the other axis. A calibration to transitions of known multipolarity shows that the ratios $R_\theta = I(\gamma 2_{fb}, \gamma 1_{all})/I(\gamma 2_{90}, \gamma 1_{all})$ lie around 1.4 and 0.6 for stretched quadrupole and dipole transitions, respectively.

III. RESULTS AND LEVEL SCHEME

The level scheme of ^{123}I based on previous work [5,25–27] and on the present results is displayed in Fig. 1. Angular distribution ratios and information on interband transitions were used to propose spin-parity assignments. The parities of the low- to medium-spin states were adopted from previous work [26]. Furthermore, for some of the new higher-spin levels, parities were determined in a recent linear polarization measurement [31]. The γ-ray energies, intensities, angular distribution ratios, adopted multipolarities, level energies, and spin-parity assignments for transitions observed in ^{123}I are listed in Table I.

The bands labeled 1 to 3 in Fig. 1 were known from previous work [26,27]. A new transition of 551.8 keV has been observed between the $23/2^+$ level of band 3 and the $19/2^+$ state of band 1. Furthermore, the multipolarity of the 346.3-, 413.8-, and 796.0-keV transitions of bands 2 and 3, respectively, was determined for the first time. The bands labeled 4 to 6 in Fig. 1 were established previously up to $I^\pi = 41/2^+$, $31/2^+$, and $47/2^-$, respectively [5,26]. In the following, only the new medium- and high-spin features of the latter bands will be discussed.

A. Medium-spin results

In the present work, bands 4 to 6 were extended to considerably higher spins and excitation energies. An irregular structure with a cascade of seven γ rays with energies of 519.5, 692.2, 747.7, 148.2, 1210.1, 258.6, and 757.7 keV was observed in coincidence with transitions from the lower part of band 4 and is labeled 4a in Fig. 1. In Fig. 2, a triple-gated coincidence spectrum is displayed, showing the newly observed transitions of this band. The observation of several crossover- and decay-out transitions from different levels support their placement. The spin assignments are based on the angular distribution results. The 692.2- and 754.3-keV transitions have angular distributions and linear polarizations [31] compatible with $M1$ and $E1$ multipolarity, respectively. Stretched quadrupole transitions are assumed to be of $E2$ character.

Band 5 was extended by one transition of 946.2 keV up to $I^\pi = 35/2^+$. Several dipole transitions linking bands 4 and 5 have also been added to the level scheme.

Negative-parity states in ^{123}I were previously known up to the $47/2^-$ level of band 6 [5]. The present experiment reveals higher-spin transitions up to $I^\pi = 59/2^-$ and an excitation energy of 10.837 MeV. A representative triple-gated coincidence spectrum for band 6 is displayed in Fig. 3.

The 801.2- and 990.5-keV transitions reported in the previous work [5] have been reordered on the basis of their relative intensities. Furthermore, the angular distribution of
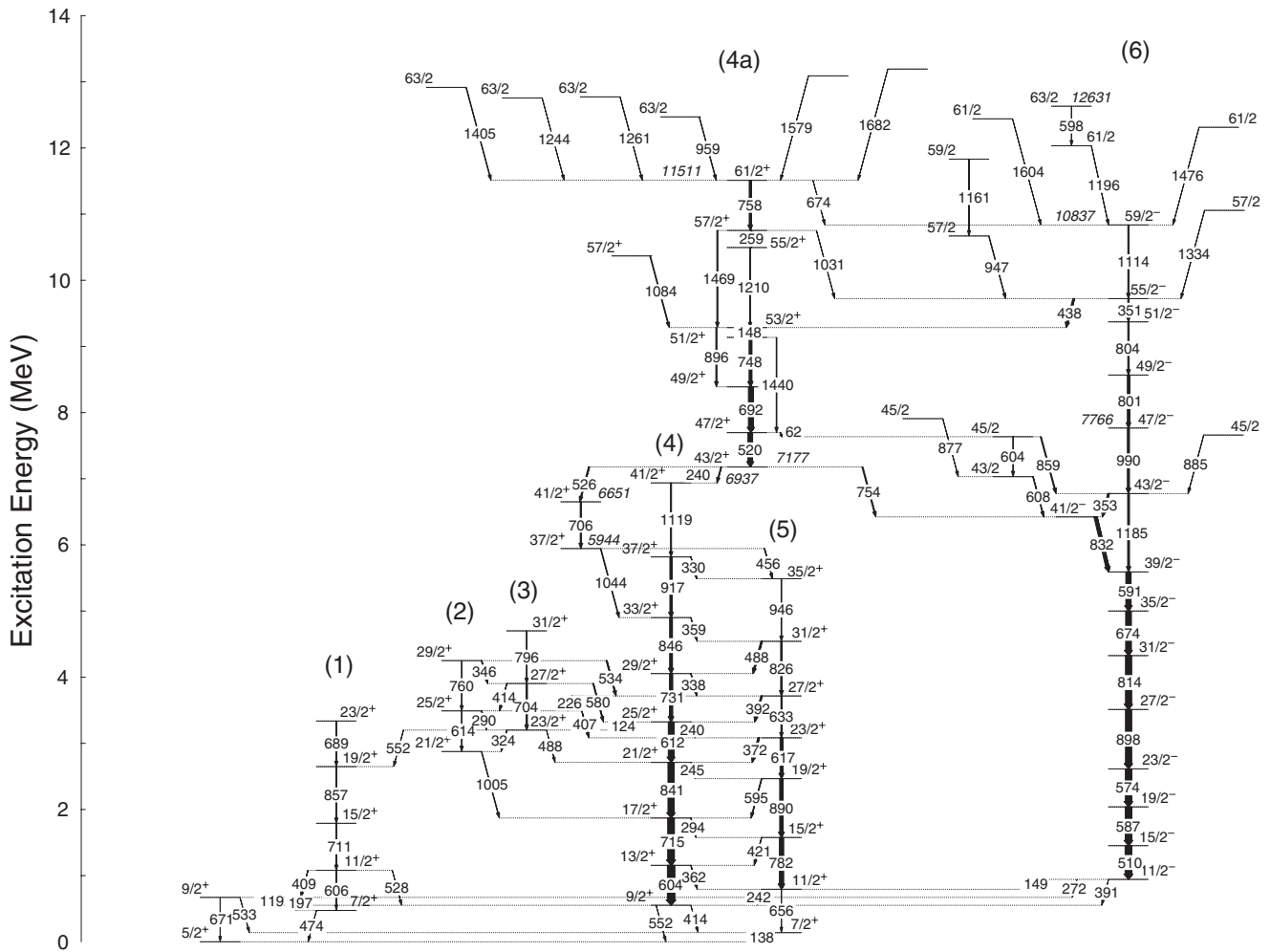
FIG. 1. The level scheme of ^{123}I.

the 990.5-keV transition is compatible with a stretched $E2$ multipolarity and, thus, $I^\pi = 47/2^-$ is assigned to the level at 7766 keV. Four γ-ray transitions with energies of 801.2, 803.8, 351.4, and 1113.8 keV have been placed in cascade above the $47/2^-$ level. The angular distributions and linear polarizations [31] of the 801.2- and 803.8-keV transitions are compatible with an $M1$ character, whereas the R_θ ratios of the 351.4- and 1113.8-keV lines show that they are of an $E2$ nature. The 438.1-keV γ ray connecting the $I^\pi = 55/2^-$ level of sequence 6 with the $53/2^+$ state of structure 4a shows the linear polarization of a stretched $E1$ transition [31]. These results establish negative parity for the new high-spin levels of band 6.

Several transitions connect the levels of structure 4a and band 6 around $I^\pi = 43/2^+$ and $61/2^+$, respectively. This explains the presence of transitions above the $43/2^+$ level of 4a in the spectrum gated by transitions from the lower part of band 6, see Fig. 3. Similarly, in Fig. 2, transitions placed above the $55/2^-$ state of band 6 are visible through the linking transition of 438.1 keV.

A group of transitions with energies of 604.0, 608.3, 859.2, and 877.2 keV has been observed to feed band 6 at the $I^\pi = 41/2^-$ and $43/2^-$ levels. These γ rays are in coincidence with

transitions placed above the $47/2^+$ state of band 4a. Therefore, a 61.5-keV transition has been tentatively placed between the $47/2^+$ and $45/2$ levels to account for the observed coincidence relationships.

B. High-spin transitions

A large number of rather weak dipole transitions are feeding into high-spin levels of sequences 4a and 6, respectively. In Figs. 4 and 5 coincidence spectra for the high-spin regions are displayed. Six high-energy transitions feed the $61/2^+$ state of structure 4a, as shown in Fig. 1. These transitions account for $\simeq$ 55 % of the feeding intensity into the $61/2^+$ state. The angular distribution analysis confirms the stretched dipole nature of the 958.7-, 1244.1-, 1261.1-, and 1404.9-keV transitions. The multipolarity of the 1579.0- and 1681.9-keV γ rays could not be determined.

The 946.9- and 1334.1-keV stretched dipole transitions populate the $I^\pi = 55/2^-$ level and three $\Delta I = 1$ γ rays with energies of 1196.3, 1476.1, and 1603.7 keV feed the $59/2^-$ state of band 6. In addition, a transition of 674.5 keV connects the $61/2^+$ level of structure 4a to the $59/2^-$ state of band 6.

TABLE I. Energies, intensities, angular distribution ratios, adopted multipolarities, level energies, and spin assignments of γ-ray transitions of ^{123}I.

Energy E_γ[a] (keV)	Intensity I_γ[b]	Intensity ratio R_θ	Multipolarity assignment	Initial level energy E_i (keV)	Spin assignment $J_i^\pi \to J_f^\pi$
61.5	–	–	$E1$	7696	$47/2^+ \to 45/2^-$
118.8	–	–	$M1$	671	$9/2^+ \to 9/2^+$
123.8	56(4)	0.53(7)	$M1$	3324	$25/2^+ \to 23/2^+$
138.2	–	0.68(4)	$M1$	138	$7/2^+ \to 5/2^+$
148.2	210(12)	0.62(4)	$M1$	9285	$53/2^+ \to 51/2^+$
149.3	–	–	$E1$	943	$11/2^- \to 11/2^+$
196.6	–	0.61(8)	$M1$	671	$9/2^+ \to 7/2^+$
225.7	76(5)	0.60(6)	$M1$	3716	$27/2^+ \to 25/2^+$
240.3[c]	72(4)	–	$M1$	3324	$25/2^+ \to 23/2^+$
240.3[c]	116(4)	–	$M1$	7177	$43/2^+ \to 41/2^+$
241.8	–	0.60(4)	$M1$	794	$11/2^+ \to 9/2^+$
245.4	78(4)	0.64(6)	$M1$	2711	$21/2^+ \to 19/2^+$
258.6	80(3)	0.74(12)	$M1$	10753	$57/2^+ \to 55/2^+$
272.3[d]	–	0.74(6)	$E1$	943	$11/2^- \to 9/2^+$
290.5	85(4)	0.75(5)	$M1$	3490	$25/2^+ \to 23/2^+$
294.4	43(20)	–	$M1$	1871	$17/2^+ \to 15/2^+$
323.9	62(4)	0.56(8)	$M1$	3200	$23/2^+ \to 21/2^+$
329.8	57(3)	0.51(7)	$M1$	5818	$37/2^+ \to 35/2^+$
338.2	78(4)	0.42(4)	$M1$	4054	$29/2^+ \to 27/2^+$
346.3	96(5)	0.53(6)	$M1$	4250	$29/2^+ \to 27/2^+$
351.4	201(10)	1.53(23)	$E2$	9723	$55/2^- \to 51/2^-$
353.1[c]	264(13)	–	$M1$	6776	$43/2^- \to 41/2^-$
358.7	37(20)	0.48(17)	$M1$	4901	$33/2^+ \to 31/2^+$
361.9	61(3)	0.57(9)	$M1$	1156	$13/2^+ \to 11/2^+$
372.0	241(12)	0.53(4)	$M1$	3083	$23/2^+ \to 21/2^+$
391.1	461(25)	0.80(4)	$E1$	943	$11/2^- \to 9/2^+$
392.4	215(10)	0.75(5)	$M1$	3716	$27/2^+ \to 25/2^+$
407.0	69(3)	0.64(8)	$M1$	3490	$25/2^+ \to 23/2^+$
409.2	42(5)	–	$M1$	1080	$11/2^+ \to 9/2^+$
413.8	42(4)	0.61(6)	$M1$	3904	$27/2^+ \to 25/2^+$
413.9	–	–	$M1$	552	$9/2^+ \to 7/2^+$
420.5	45(3)	–	$M1$	1576	$15/2^+ \to 13/2^+$
438.1[d]	266(14)	0.80(6)	$E1$	9723	$55/2^- \to 53/2^+$
456.3	81(4)	–	$M1$	5944	$37/2^+ \to 35/2^+$
474.3	–	0.43(9)	$M1$	474	$7/2^+ \to 5/2^+$
487.6	108(5)	–	$M1$	4542	$31/2^+ \to 29/2^+$
488.5	113(7)	0.63(7)	$M1$	3200	$23/2^+ \to 21/2^+$
509.5	1000(47)	1.30(4)	$E2$	1453	$15/2^- \to 11/2^-$
519.5	706(35)	1.54(6)	$E2$	7696	$47/2^+ \to 43/2^+$
526.3	162(8)	–	$M1$	7177	$43/2^+ \to 41/2^+$
528.0[c]	–	–	$M1$	1080	$11/2^+ \to 9/2^+$
532.7	–	–	$M1$	671	$9/2^+ \to 7/2^+$
534.4	151(8)	–	$M1$	4250	$29/2^+ \to 27/2^+$
551.8	45(4)	–	$E2$	3200	$23/2^+ \to 19/2^+$
552.1	–	1.37(6)	$E2$	552	$9/2^+ \to 5/2^+$
574.1	919(46)	1.42(4)	$E2$	2613	$23/2^- \to 19/2^-$
580.5	121(8)	–	$M1$	3904	$27/2^+ \to 25/2^+$
586.6	952(48)	1.36(6)	$E2$	2039	$19/2^- \to 15/2^-$
590.8	789(40)	1.40(5)	$E2$	5591	$39/2^- \to 35/2^-$
595.3	86(4)	–	$M1$	2466	$19/2^+ \to 17/2^+$
598.1	36(3)	0.49(13)	$M1$ or $E1$	12631	$63/2 \to 61/2$
603.7	1085(54)	–	$E2$	1156	$13/2^+ \to 9/2^+$
604.0[c]	–	–	$M1$ or $E1$	7635	$45/2 \to 43/2$
605.8	–	1.23(5)	E2	1080	$11/2^+ \to 7/2^+$
608.3	80(5)	–	$M1$ or $E1$	7031	$43/2 \to 41/2^-$

TABLE I. (*Continued.*)

Energy E_γ [a] (keV)	Intensity I_γ [b]	Intensity ratio R_θ	Multipolarity assignment	Initial level energy E_i (keV)	Spin assignment $J_i^\pi \to J_f^\pi$
612.3	824(39)	1.36(7)	$E2$	3324	$25/2^+ \to 21/2^+$
614.4	89(6)	–	$E2$	3490	$25/2^+ \to 21/2^+$
617.4	401(21)	1.70(23)	$E2$	3083	$23/2^+ \to 19/2^+$
632.7	143(7)	1.12(20)	$E2$	3716	$27/2^+ \to 23/2^+$
655.7	–	1.31(13)	$E2$	794	$11/2^+ \to 7/2^+$
670.9	–	1.17(8)	$E2$	671	$9/2^+ \to 5/2^+$
674.5	18(3)	–	$E1$	11511	$61/2^+ \to 59/2^-$
674.5	838(40)	1.44(6)	$E2$	5000	$35/2^- \to 31/2^-$
689.3	89(7)	–	$E2$	3337	$23/2^+ \to 19/2^+$
692.2[d]	732(40)	0.60(7)	$M1$	8389	$49/2^+ \to 47/2^+$
704.3	171(10)	1.41(13)	$E2$	3904	$27/2^+ \to 23/2^+$
706.2	183(8)	1.44(10)	$E2$	6651	$41/2^+ \to 37/2^+$
711.2	97(5)	–	$E2$	1791	$15/2^+ \to 11/2^+$
714.9	1000(51)	1.30(5)	$E2$	1871	$17/2^+ \to 13/2^+$
730.6	465(24)	1.70(19)	$E2$	4054	$29/2^+ \to 25/2^+$
747.7	410(22)	0.68(10)	$M1$	9136	$51/2^+ \to 49/2^+$
754.3[d]	163(9)	0.62(7)	$E1$	7177	$43/2^+ \to 41/2^-$
757.7	319(14)	1.38(6)	$E2$	11511	$61/2^+ \to 57/2^+$
760.1	82(5)	–	$E2$	4250	$29/2^+ \to 25/2^+$
782.4	612(30)	1.56(11)	$E2$	1576	$15/2^+ \to 11/2^+$
796.0	98(6)	1.50(13)	$E2$	4700	$31/2^+ \to 27/2^+$
801.2[d]	308(16)	0.53(15)	$M1$	8568	$49/2^- \to 47/2^-$
803.8[d]	211(9)	0.64(8)	$M1$	9371	$51/2^- \to 49/2^-$
814.1	889(45)	1.38(4)	$E2$	4326	$31/2^- \to 27/2^-$
825.8	223(13)	1.12(10)	$E2$	4542	$31/2^+ \to 27/2^+$
831.6	492(23)	0.51(4)	$M1$	6423	$41/2^- \to 39/2^-$
840.7	921(49)	1.20(6)	$E2$	2711	$21/2^+ \to 17/2^+$
846.3	417(22)	1.50(10)	$E2$	4901	$33/2^+ \to 29/2^+$
856.8	93(10)	–	$E2$	2648	$19/2^+ \to 15/2^+$
859.2	158(8)	0.60(9)	$M1$ or $E1$	7635	$45/2 \to 43/2^-$
877.2	38(3)	0.49(6)	$M1$ or $E1$	7908	$45/2 \to 43/2^-$
884.6	40(4)	0.58(8)	$M1$ or $E1$	7660	$45/2 \to 43/2^-$
889.7	524(32)	1.40(7)	$E2$	2466	$19/2^+ \to 15/2^+$
895.9	174(12)	1.69(21)	$E2$	9285	$53/2^+ \to 49/2^+$
898.3	892(44)	1.58(10)	$E2$	3512	$27/2^- \to 23/2^-$
917.3	340(18)	1.60(12)	$E2$	5818	$37/2^+ \to 33/2^+$
946.2	98(5)	–	$E2$	5488	$35/2^+ \to 31/2^+$
946.9	79(6)	0.64(6)	$M1$ or $E1$	10670	$57/2 \to 55/2^-$
958.7	72(4)	0.43(8)	$M1$ or $E1$	12470	$63/2 \to 61/2^+$
990.5	315(15)	1.42(10)	$E2$	7766	$47/2^- \to 43/2^-$
1005.3	84(4)	1.24(8)	$E2$	2876	$21/2^+ \to 17/2^+$
1030.6	34(3)	–	$E1$	10753	$57/2^+ \to 55/2^-$
1043.8	106(5)	1.34(13)	$E2$	5944	$37/2^+ \to 33/2^+$
1083.5	116(7)	1.26(11)	$E2$	10368	$57/2^+ \to 53/2^+$
1113.8	171(10)	1.20(4)	$E2$	10837	$59/2^- \to 55/2^-$
1118.8	162(10)	1.40(7)	$E2$	6937	$41/2^+ \to 37/2^+$
1161.1	51(4)	0.78(8)	$M1$ or $E1$	11831	$59/2 \to 57/2$
1184.7	283(12)	1.48(6)	$E2$	6776	$43/2^- \to 39/2^-$
1196.3	44(5)	0.54(10)	$M1$ or $E1$	12033	$61/2 \to 59/2^-$
1210.1	87(4)	0.74(8)	$M1$	10495	$55/2^+ \to 53/2^+$
1244.1	32(4)	0.71(23)	$M1$ or $E1$	12755	$63/2 \to 61/2^+$
1261.1	21(5)	0.57(15)	$M1$ or $E1$	12772	$63/2 \to 61/2^+$
1334.1	18(5)	0.58(11)	$M1$ or $E1$	11057	$57/2 \to 55/2^-$
1404.9	23(10)	0.60(11)	$M1$ or $E1$	12916	$63/2 \to 61/2^+$
1439.9	98(9)	1.21(14)	$E2$	9136	$51/2^+ \to 47/2^+$
1468.7	158(7)	1.46(9)	$E2$	10753	$57/2^+ \to 53/2^+$

TABLE I. (*Continued.*)

Energy E_γ [a] (keV)	Intensity I_γ [b]	Intensity ratio R_θ	Multipolarity assignment	Initial level energy E_i (keV)	Spin assignment $J_i^\pi \to J_f^\pi$
1476.1	10(2)	0.50(18)	$M1$ or $E1$	12313	$61/2 \to 59/2^-$
1579.0	15(3)	–	–	13090	$- \to 61/2^+$
1603.7	11(2)	0.49(16)	$M1$ or $E1$	12440	$61/2 \to 59/2^-$
1681.9	12(2)	–	–	13193	$- \to 61/2^+$

[a]The uncertainties lie between 0.2 and 0.6 keV, depending on intensity.

[b]Intensities for γ rays originating from negative- and positive-parity states are normalized to the 509.5-keV and 714.9-keV transitions, respectively, with $I_\gamma = 1000$.

[c]Measurement of intensity or intensity ratio not possible due to presence of γ rays of overlaping energy.

[d]Electric or magnetic nature of the transition has been determined from the linear polarization measurement of Ref. [31].

The three high-energy transitions account for $\simeq 38\%$ of the feeding into the $59/2^-$ state.

The parities of the states above the $I^\pi = 55/2^-, 59/2^-$, and $61/2^+$ levels could not be determined.

IV. DISCUSSION

In this section, the new features of the ^{123}I level scheme, established in the present work, will be discussed. Configurations for the high-spin states are explored within the framework of the CNS model. Of particular interest are the noncollective aligned and antialigned states as well as the core-breaking excitations decaying into these levels.

A. Cranked Nilsson-Strutinsky calculations

Calculations were performed within the framework of the configuration-dependent CNS formalism [32–34]. Pairing was not included. Hence, the results are relevant at high spin, where pairing is quenched. Within this approach, bands are calculated for fixed configurations, specified by the number of particles in different oscillator shells, N_{osc}, with both signatures. Furthermore, within each N_{osc} shell, a division is made into orbitals having their main amplitudes in the intruder high-j and in the other j-shells, respectively. A search for the lowest-energy states at a given spin is made within a mesh of the deformation space ($\varepsilon_2, \varepsilon_4, \gamma$), treating the collective and noncollective states on an equal footing. For the parameters κ and μ, defining the $l \cdot s$ and l^2 strengths of the modified oscillator potential, the so-called $A = 110$ parameters [35] are used, which give a good description of the smooth terminating bands in the neutron-deficient $Z = 49$–54 nuclei [32].

The Lublin-Strasbourg drop (LSD) model [36] is employed for the macroscopic energy, with the rigid-body moment of inertia calculated with a radius parameter of $r_0 = 1.16$ fm and a diffuseness of $a = 0.6$ fm [34].

The calculated configurations are labeled relative to the ^{114}Sn core by the shorthand notation $[p_1, n_1]$, where p_1 and n_1 denote the number of protons and neutrons in $h_{11/2}$ orbitals, respectively. The remaining protons outside the core are distributed in the orbitals of $g_{7/2}d_{5/2}$ character and the remaining neutrons in the $d_{3/2}s_{1/2}$ orbitals. The calculations indicate that configurations involving particle-hole excitations
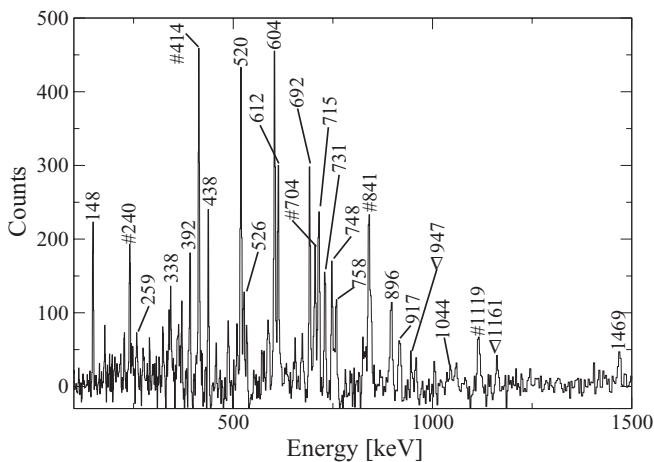

FIG. 2. Summed triple-gated γ-ray coincidence spectrum for bands 4 and 4a, created with a gate on the 138-keV transition and with double gates from the list of 414-, 604-, 715-, 841-, and 846-keV γ rays. The peaks marked with $\triangledown$ signs belong to band 6. Hash-marked peaks are unresolved doublets.
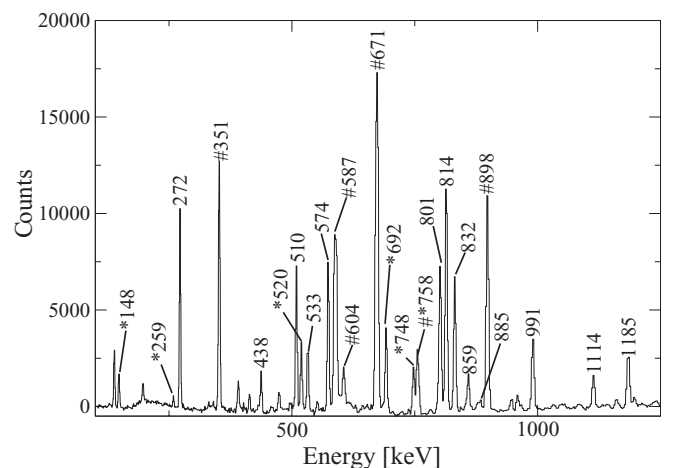

FIG. 3. Summed triple-gated γ-ray coincidence spectrum obtained with gates on all transitions between 272 and 591 keV in band 6. The peaks marked with asterisks correspond to transitions of band 4a. Hash-marked peaks are unresolved doublets.
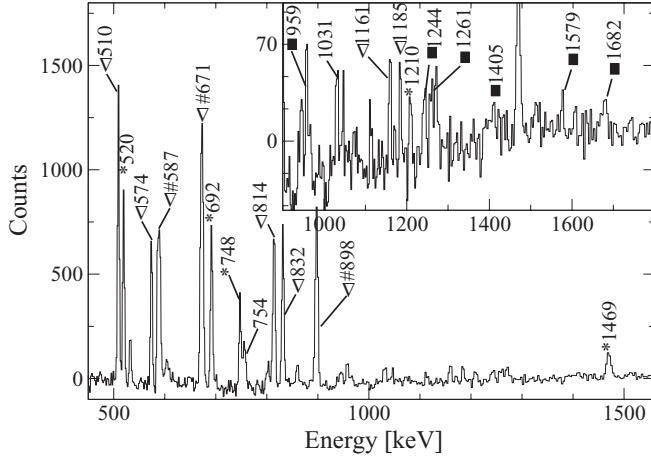
FIG. 4. Summed triple-gated γ-ray coincidence spectrum showing high-spin transitions, marked by filled squares, feeding the $61/2^+$ state created with a gate on the 758-keV γ ray, a second gate from the list of 272 and 587 keV, and a third one from the list of 574, 591, and 148 keV. The peaks marked with $\triangledown$ signs belong to low-lying states of band 6. Asterisks denote transitions of band 4a. Hash-marked peaks are unresolved doublets.

from the $N = 64$ neutron core become important for the highest-spin states.

B. Aligned and antialigned terminating states

The experimental excitation energies of structure 4a relative to a rotating liquid drop reference above $I^\pi = 41/2^+$ are presented in the upper panel of Fig. 6. The favored states with $I^\pi = 47/2^+$, $53/2^+$, and $61/2^+$ are highlighted by open squares.
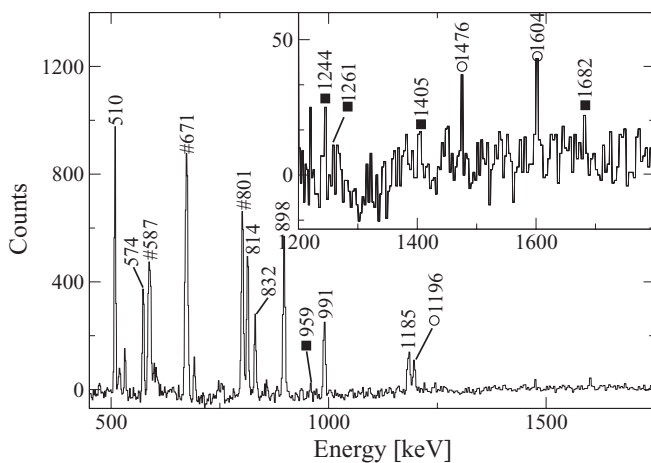
FIG. 5. Summed triple-gated γ-ray coincidence spectrum showing high-spin transitions feeding the $59/2^-$ level, generated with a gate on the 1114-keV γ ray, a second one from the list of 272 and 587 keV, and a third gate from the list of 574 and 591 keV. The high-energy transitions feeding into the $59/2^-$ state are marked with open circles. Closed squares denote high-energy transitions feeding the $61/2^+$ state. Hash-marked peaks are unresolved doublets.
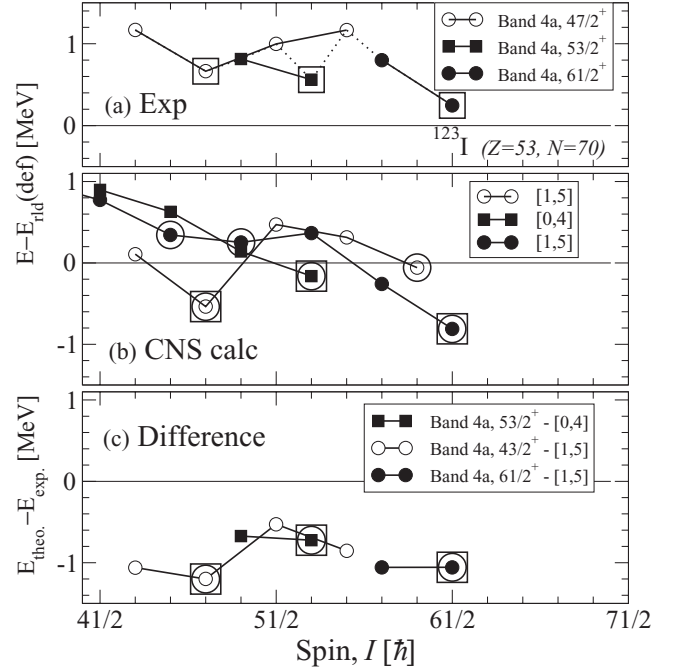

FIG. 6. Excitation energies relative to a rotating liquid drop for low-lying observed (a) and calculated (b) positive-parity states in ^{123}I. The difference between experiment and calculations is given in (c). Aligned states are encircled; open squares indicate the observed and corresponding calculated states, which appear especially low in energy.

Fully aligned high-spin states within the valence space can be formed by coupling three protons outside the ^{114}Sn core to

$$\pi[(g_{7/2}d_{5/2})^2_6 h_{11/2}]_{23/2^-}$$
$$\text{or to } \pi[(g_{7/2}d_{5/2})^3]_{17/2^+}$$

configurations. These configurations are illustrated in the tilted Fermi surface diagram in the upper panel of Fig. 7. They can couple with the favored aligned neutron configurations, see middle panel of Fig. 7,

$$\nu[(h_{11/2})^5_{35/2}(d_{3/2}s_{1/2})_{3/2}]_{19^-}$$
$$\text{and } \nu[(h_{11/2})^4_{16}(d_{3/2}s_{1/2})^2_2]_{18^+},$$

respectively, to aligned states with $I^\pi = 53/2^+$, $55/2^-$, $59/2^-$, and $61/2^+$.

The results obtained from the CNS calculations for the positive-parity states are given in the middle panel of Fig. 6. Favored states with $I^\pi = 53/2^+$ and $61/2^+$ are well reproduced. These states are built from the fully aligned proton and neutron configurations listed above and illustrated in Fig. 7.

The favored state with $I^\pi = 47/2^+$ probably has the [1,5] configuration, as displayed in the middle panel of Fig. 6. It is calculated low in energy for $I^\pi = 47/2^+$ at a deformation of $\varepsilon_2 = 0.18$; i.e., $I^\pi_p = 23/2^-$ and $I^\pi_n = 12^-$, see upper and lower panels of Fig. 7, where a neutron is relocated from the $m_i = +3/2$ to the $m_i = -11/2$ orbital relative to the fully aligned $I^\pi_n = 19^-$ state. This [1,5] configuration with signature $\alpha = -1/2$ corresponds to an oblate shape, with the spin of one valence nucleon aligned in the direction opposite to the total angular momentum vector [37]. The $\alpha = -1/2$ branch is
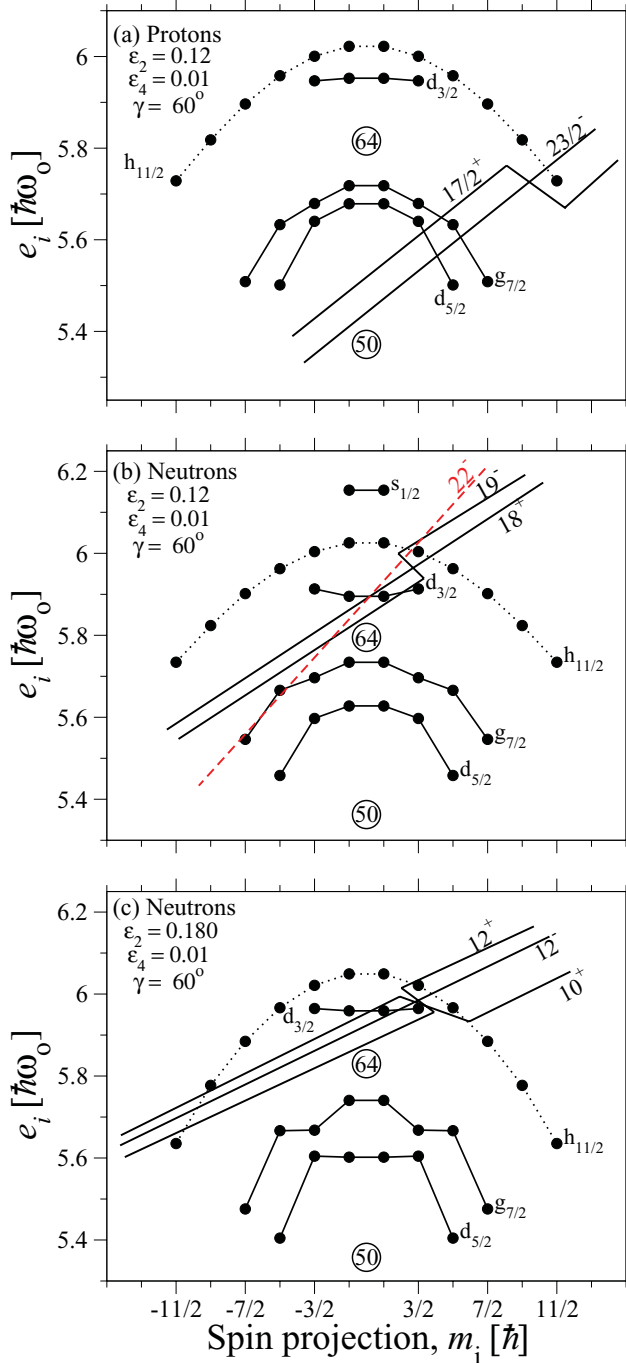
FIG. 7. (Color online) Favored aligned states for $Z = 53$ configurations (a) and $N = 70$ configurations with all neutrons aligned (b) and with one neutron antialigned (c). Configurations with four $h_{11/2}$ neutrons result in $I_n^\pi = 18^+$ and 10^+ states. $I_n^\pi = 22^-$, 19^-, and 12^- states are formed with five $h_{11/2}$ neutrons, however with one hole in the $N = 64$ core for the $I_n^\pi = 22^-$ state. All six valence neutrons are in the $h_{11/2}$ shell in the 12^+ state. The structures were calculated for deformations close to their respective equilibrium, as given in the three panels.

The difference between experiment and calculations is displayed in the lower panel of Fig. 6. The calculated energies are approximately 1 MeV low compared to the observed values. This difference lies within the same range as observed for terminating bands in this as well as in other mass regions [11,34] and should be further explored theoretically.

The negative-parity yrast band 6 terminates at $I^\pi = 59/2^-$. This is the maximum spin that can be generated for negative parity by aligning all nine particles outside the ^{114}Sn core. The configuration of this maximally aligned state is obtained by combining the $23/2^-$ and 18^+ states listed above, with the occupancy of the valence orbitals illustrated in the tilted Fermi surface diagram of Fig. 7.

The calculated energies for the corresponding configuration are found in the middle panel of Fig. 8, which agree rather well with the experimental data displayed in the upper panel. The difference between experiment and calculations is shown in the lower panel; again, the differences lie in the range of $\simeq 1$ MeV.

At lower spin, favored states with $I^\pi = 43/2^-$ and $47/2^-$ can be identified in both, the data and the calculations, see upper and middle panels of Fig. 8. A possible configuration that can be assigned to the $43/2^-$ state is $\pi[(g_{7/2}d_{5/2})_6^2 h_{11/2}]_{23/2^-} \otimes \nu[(h_{11/2})_8^4 (d_{3/2}s_{1/2})_2^2]_{10^+}$ or [1,4]. The neutron configuration, illustrated in the lower panel of Fig. 7, can be understood as resulting from the transfer of one $h_{11/2}$ neutron from the $m_i = +5/2$ to the $m_i = -11/2$ orbital with respect to the fully aligned $I_n^\pi = 18^+$ state, shown in the middle panel. Similarly, a favored oblate $47/2^-$ state is calculated in the [1,6]
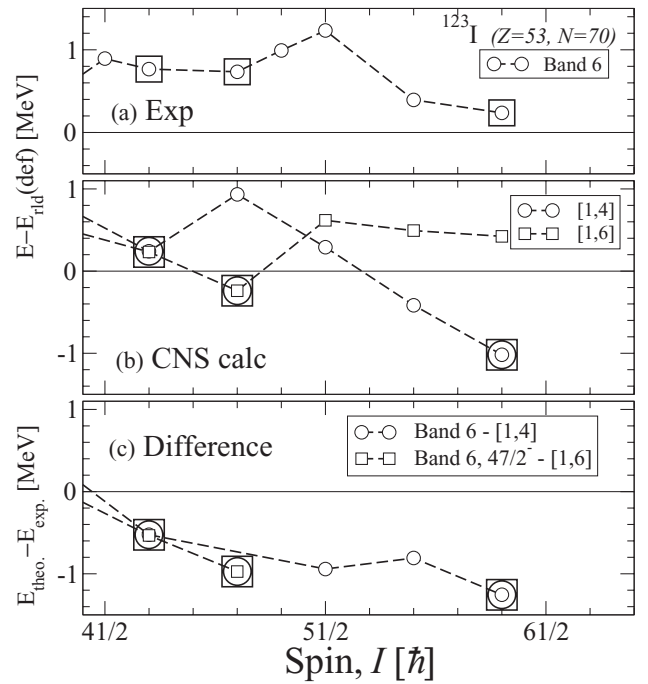

FIG. 8. Excitation energies relative to a rotating liquid drop reference for low-lying observed (a) and calculated (b) negative-parity states in ^{123}I. The difference between experiment and calculations is shown in (c). Aligned states are encircled; open squares indicate the observed and corresponding calculated states, which appear especially low in energy.
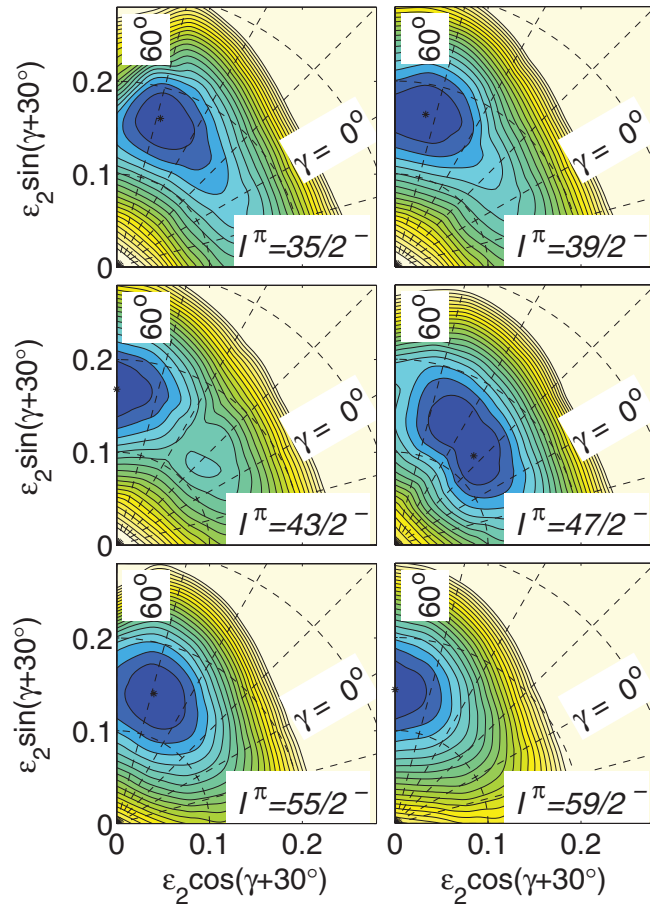
less favored in energy for $I > 51/2$ and has no experimental counterpart. The favored signature, $\alpha = +1/2$, of the [1,5] configuration is assigned to the high-spin states of band 4a.

FIG. 9. (Color online) Calculated PES for ^{123}I in the spin range $I = 35/2$–$59/2$ for the $\pi h_{11/2}\nu(h_{11/2})^4$ configuration which is assigned to observed states of band 6. The contour line separation is 0.1 MeV.

configuration with one antialigned neutron in the $h_{11/2}$ shell. This level is formed from the $I_n^\pi = 19^-$ state, see middle panel of Fig. 7, when one $m_i = +3/2$, $d_{3/2}$ neutron is relocated to the $m_i = -11/2$, $h_{11/2}$ orbital, see lower panel. It can naturally be assigned to the low-lying $47/2^-$ state observed in band 6, see Fig. 8. This configuration assignment is further supported by the fact that no low-lying $47/2^-$ state is calculated in the [1,4] configuration.

Potential energy surfaces (PES) for the configuration [1,4] are displayed in Fig. 9. At low spin, up to $I^\pi = 39/2^-$, a small collectivity is observed ($\gamma \approx 45°$ for $I^\pi = 35/2^-$, $39/2^-$). A noncollective oblate minimum with $\gamma = 60°$ appears for $I^\pi = 43/2^-$, which is a state with one antialigned neutron, as discussed above. At $I^\pi = 47/2^-$, this minimum is observed with $\gamma = 15°$. With increasing spin it migrates gradually toward lower collectivity and, finally, becomes oblate at $I^\pi = 59/2^-$, where the configuration terminates. The shift of the minimum in the PES calculations toward smaller deformation with increasing spin is correlated with a decrease in the occupancy of high-Ω orbitals driving the nucleus toward larger deformation. For example, both of the strongly deformation-driving $m_i = \pm 11/2$ states are occupied in the

noncollective $43/2^-$ level while only the $m_i = +11/2$ orbital is involved in the fully aligned $59/2^-$ state.

C. Core-excited states

Several high-energy γ rays feeding the maximally aligned states at $I^\pi = 59/2^-$ and $61/2^+$ have been observed. However, the parity of these states could not be determined. Their excitation energies relative to a rotating liquid drop reference are displayed in the upper panel of Fig. 10. As discussed above, the maximally aligned terminating states are generated by aligning the angular momenta of all the valence nucleons outside the ^{114}Sn core. To generate higher angular momenta, neutrons from the orbitals of $g_{7/2}d_{5/2}$ character below the $N = 64$ neutron shell gap have to be excited to the $d_{3/2}s_{1/2}$ or $h_{11/2}$ orbitals above the gap.

A systematic investigation has been carried out for the core-excited configurations with one to four neutrons excited across the $N = 64$ gap. Examples from these calculations are found in the lower panel of Fig. 10. In this analysis it is necessary to distinguish between $N_{osc} = 4$ $g_{7/2}d_{5/2}$ and $d_{3/2}s_{1/2}$ orbitals, which turns out to be rather straightforward
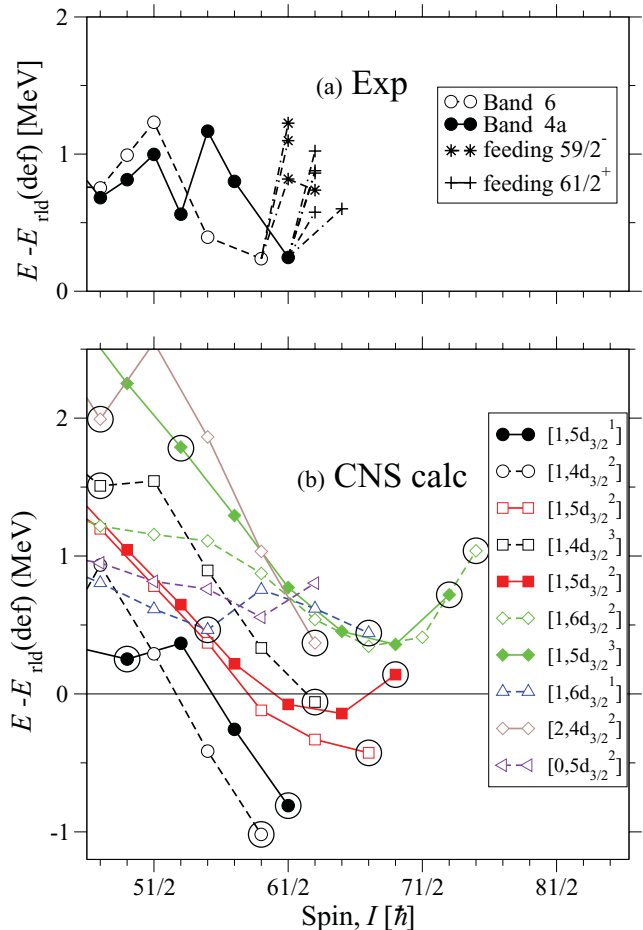

FIG. 10. (Color online) Experimental (a) and calculated (b) excitation energies relative to a rotating liquid drop reference for the configurations of the observed maximally aligned states and for the configurations feeding these levels.

at the small deformations of these high-spin configurations. In the configuration labels, not only the number of neutrons in $h_{11/2}$ orbitals, but also the number of neutrons in $d_{3/2}s_{1/2}$ orbitals, which are dominated by the $d_{3/2}$ shell, is specified. Thus, e.g., the fully aligned $59/2^-$ and $61/2^+$ states are labeled as $[1, 4d_{3/2}^2]$ and $[1, 5d_{3/2}^1]$, respectively.

With a single neutron excitation across the $N = 64$ gap, the configurations $[1,6d_{3/2}^1]$, $[1,5d_{3/2}^2]$, and $[1,4d_{3/2}^3]$ are formed, depending on how the valence particles are distributed over the $h_{11/2}$ and $d_{3/2}s_{1/2}$ orbitals. In these cases, two rather closely-lying bands are formed depending on the signature of the $g_{7/2}d_{5/2}$ hole. This is illustrated for the $[1,5d_{3/2}^2]$ configuration in Fig. 10(b), whereas only the favored signature is shown for the other two configurations. The distribution of the neutrons in the $[1,5d_{3/2}^2]$ configuration, which terminates at $I^\pi = 67/2^+$, is illustrated in Fig. 7(b). The rotational bands resulting from two holes in the $N = 64$ neutron core generally lie at a somewhat higher energy as demonstrated for the $[1,6d_{3/2}^2]$ and $[1,5d_{3/2}^3]$ configurations in Fig. 10, which are about equally favored in energy.

Another possibility is to consider configurations with either no or two $h_{11/2}$ protons. In order to feed the terminating $I^\pi = 59/2^-$ and $61/2^+$ states, they have to be combined with high-spin neutron configurations to result in states with $I_{\max} > 59/2$. However, these states lie rather high in energy, as exemplified by the $[2,4d_{3/2}^2]$ and $[0,5d_{3/2}^2]$ configurations in Fig. 10.

The configurations drawn in Fig. 10 are just examples of the low-lying core-excited states. However, other calculated levels lie in the order 1.5 MeV or more above the terminating $I^\pi = 59/2^-$ and $61/2^+$ states, when drawn, as in Fig. 10, with a reference subtracted. The observed states, displayed in the upper panel of the figure, appear at a lower energy, indicating that the $N = 64$ neutron gap is calculated somewhat too large with the present parameters.

High-spin states in neighboring ^{125}I were recently established up to $I = 95/2$ [11]. However, a pattern of several core-excited levels feeding the maximally aligned states was not observed in this nucleus. The configuration $\pi(g_{7/2}d_{5/2})^2 h_{11/2} \otimes \nu(h_{11/2})^6_{18}(s_{1/2}d_{3/2})^2_2$ was assigned to the maximally aligned state in ^{125}I. Within this valence-space configuration one neutron can be excited across the $N = 64$ neutron shell gap from the $g_{7/2}d_{5/2}$ to $d_{3/2}s_{1/2}$ orbitals leading to a maximum addition of $4\hbar$ to the maximally aligned state. Further excitations from the $g_{7/2}d_{5/2}$ to the $d_{3/2}s_{1/2}$ or $h_{11/2}$ orbitals lead to antialigned pairs. This implies that the excitations from the $N = 64$ core to the valence orbitals are not favored due to a rather limited addition of angular momentum.

At higher excitation energies, it is favorable to excite particles from the $g_{7/2}d_{5/2}$ to the $h_{9/2}f_{7/2}$ and $i_{13/2}$ orbitals across the $N = 82$ neutron shell gap, leading to highly deformed bands in ^{125}I [20]. Deformed bands of this type have also been observed in ^{123}I. They will be discussed in a forthcoming publication [28].

V. SUMMARY

The level scheme of ^{123}I has been extended for both parities up to the maximum spin available within the valence space. At high spin, this nucleus develops into structures with a weakly deformed oblate shape. Band-terminating states have been observed at $I^\pi = 53/2^+$, $59/2^-$, and $61/2^+$. These states are favored in energy relative to a rotating liquid drop reference. Their structure is well understood from comparisons with CNS calculations. In addition, lower-lying states with $I^\pi = 43/2^-$, $47/2^-$, and $47/2^+$ have been tentatively assigned as noncollective states where one particle is antialigned.

Several dipole transitions of energies in the range of 1.0–1.7 MeV have been observed, feeding the energetically favored $I^\pi = 61/2^+$ and $59/2^-$ terminating states. The fact that these states are fed by several transitions with intensities which are much smaller than the intensity of the transition de-exciting the state is a fingerprint that they correspond to the termination of a configuration. CNS calculations indicate that these transitions originate from configurations involving a core-breaking neutron particle-hole excitation, from the $g_{7/2}d_{5/2}$ to the $d_{3/2}s_{1/2}$ or $h_{11/2}$ orbitals across the semimagic $N = 64$ neutron shell gap.

[1] E. S. Paul *et al.*, J. Phys. G **18**, 837 (1992).

[2] M. P. Waring *et al.*, Phys. Rev. C **48**, 2629 (1993).

[3] Y. Liang *et al.*, Phys. Rev. C **45**, 1041 (1992).

[4] Y. Liang *et al.*, Phys. Rev. C **44**, R578 (1991).

[5] D. L. Balabanski *et al.*, Phys. Rev. C **56**, 1629 (1997).

[6] C.-B. Moon and T. Komatsubara, J. Korean Phys. Soc. **45**, L791 (2004).

[7] E. S. Paul *et al.*, Phys. Rev. C **45**, R2531 (1992).

[8] S. Törmänen *et al.*, Nucl. Phys. A **613**, 282 (1997).

[9] E. S. Paul *et al.*, Phys. Rev. C **59**, 1984 (1999).

[10] E. S. Paul *et al.*, J. Phys. G **19**, 913 (1993).

[11] P. Singh *et al.*, Phys. Rev. C **82**, 034301 (2010).

[12] J. Simpson *et al.*, Phys. Lett. B **327**, 187 (1994).

[13] E. S. Paul *et al.*, Phys. Rev. C **79**, 044324 (2009).

[14] A. O. Evans *et al.*, Phys. Rev. C **73**, 064303 (2006).

[15] M. Mustafa *et al.*, Phys. Rev. C **84**, 054320 (2011).

[16] A. O. Evans *et al.*, Phys. Rev. Lett. **92**, 252502 (2004).

[17] N. Nica *et al.*, Phys. Rev. C **64**, 034313 (2001).

[18] M. A. Riley *et al.*, Phys. Scr., T **125**, 123 (2006).
[19] A. K. Singh *et al.*, Phys. Rev. C **70**, 034315 (2004).
[20] P. Singh *et al.*, Phys. Rev. C **84**, 024316 (2011).
[21] A. Al-Khatib *et al.*, Phys. Rev. C **83**, 024306 (2011).
[22] C. Ronn Hansen *et al.*, Phys. Rev. C **76**, 034311 (2007).
[23] A. Al-Khatib *et al.*, Phys. Rev. C **74**, 014305 (2006).
[24] S. Nag *et al.*, Phys. Rev. C **85**, 14310 (2012).
[25] R. Goswami, B. Sethi, P. Banerjee, and R. K. Chattopadhyay, Phys. Rev. C **47**, 1013 (1993).
[26] S.-Y. Wang *et al.*, J. Phys. G **32**, 283 (2006).
[27] Y.-X. Zhao, T. Komatsubara, Y.-J. Ma, Y.-H. Zhang, S.-Y. Wang, Y.-Z. Liu, and K. Furuno, Chin. Phys. Lett. **26**, 082301 (2009).
[28] P. Singh *et al.* (to be published).
[29] I. Y. Lee, Nucl. Phys. A **520**, 641c (1990).
[30] D. C. Radford, Nucl. Instrum. Methods Phys. Res. A **361**, 297 (1995).
[31] P. Singh (private communication).
[32] A. V. Afanasjev, D. B. Fossan, G. J. Lane, and I. Ragnarsson, Phys. Rep. **322**, 1 (1999).
[33] T. Bengtsson and I. Ragnarsson, Nucl. Phys. A **436**, 14 (1985).
[34] B. G. Carlsson and I. Ragnarsson, Phys. Rev. C **74**, 011302(R) (2006).
[35] Jing-ye Zhang, N. Xu, D. B. Fossan, Y. Liang, R. Ma, and E. S. Paul, Phys. Rev. C **39**, 714 (1989).
[36] K. Pomorski and J. Dudek, Phys. Rev. C **67**, 044316 (2003).
[37] I. Ragnarsson and T. Bengtsson, Nucl. Phys. A **447**, 251c (1985).